



ELSEVIER

Marine and Petroleum Geology 19 (2002) 1151–1168

Marine and
Petroleum Geology

www.elsevier.com/locate/marpetgeo

Maturity-related variation in the bulk-transformation kinetics of a suite of compositionally related New Zealand coals

Steve Killops^{a,*}, Dan Jarvie^b, Richard Sykes^a, Rob Funnell^a

^a*Institute of Geological and Nuclear Sciences, P.O. Box 30368, Lower Hutt, New Zealand*

^b*Humble Geochemical Services, P.O. Box 789, Humble, TX 77347, USA*

Received 3 August 2000; received in revised form 10 August 2001; accepted 30 August 2001

Abstract

Bulk HI transformation kinetics were determined by open-system pyrolysis for a suite of compositionally related Late Cretaceous to Paleocene coals from Tara-1 well, Great South Basin, New Zealand. These coals span a maturity range encompassing the onset of significant oil generation and expulsion. Kinetic parameters were also obtained for one of the immature samples following artificial maturation by hydrous pyrolysis. Kinetic models were based on three modes of optimisation of kinetic parameters: discrete- E_{act} distribution with single variable A value; discrete- E_{act} distribution with fixed A (10^{14} s^{-1}); and Gaussian- E_{act} distribution with single variable A value. HI transformation-rate vs. temperature envelopes for the naturally matured coals exhibited an abrupt jump to higher temperature near $\text{Rank}(S_r)$ 12.5, apparently coinciding with the onset of significant paraffinic oil expulsion, for all optimisation modes. The artificially matured sample does not predict this shift in transformation envelopes, which suggests that certain of the reactions that occur under natural maturation do not occur during laboratory pyrolysis. The structural rearrangements occurring up to the expulsion threshold, some or all of which are responsible for the increase in HI up to $\text{Rank}(S_r) \sim 11$, are not manifested in changes in HI transformation-rate envelopes. However, the presence of adsorbed bitumen may mask the influence of structural rearrangements during optimisation of the kinetic data, which could explain the behaviour of the transformation-rate envelopes in the $\text{Rank}(S_r)$ 11.0–12.5 range obtained from the discrete- E_{act} free- A optimisation. This behaviour involves a regression in transformation-rate envelopes to lower temperatures as the amount of retained bitumen increases prior to expulsion. The almost perfect nesting of transformation-rate envelopes subsequent to oil expulsion suggests either that any further structural rearrangement does not produce a significant change in the A and E_{act} distributions of hydrocarbon-generating bonds, or that the expulsion drastically reduces the degree of further rearrangements involving hydrocarbon-generating moieties within the kerogen. It follows that kinetic parameters for immature coals should not be considered ideal for modelling the whole phase of hydrocarbon generation. Nevertheless, the kinetic parameters for the least mature Tara coal ($\text{Rank}(S_r) \sim 8.5$) reproduced the normalised HI trend for the entire suite of coals with reasonable accuracy over the maturity range considered ($\text{Rank}(S_r) \sim 8.5$ –15.0), only slightly underestimating conversion at the lower maturity levels and overestimating it slightly at the higher levels.

© 2002 Elsevier Science Ltd. All rights reserved.

Keywords: Bitumen; Coal; Kinetics; Oil expulsion; Pyrolysis; Rank; Structural rearrangement

1. Introduction

Modelling petroleum generation from coals (and type III kerogens in general) presents problems additional to those encountered with marine source rocks, apparently related to structural rearrangements of the macromolecular network. One of the problems is estimating the initial petroleum potential. Routine Rock-Eval analysis of coals provides HI

values that appear to increase with maturity up to a vitrinite reflectance (VR) of ca. 0.7–0.8% ($\text{Rank}(S_r) \sim 11$ –12) before declining with the onset of significant petroleum generation and expulsion (Bostick & Daws, 1994; Durand & Paratte, 1983; Suggate & Boudou, 1993; Teichmüller & Durand, 1983). This phenomenon is particularly well demonstrated in suites of samples in which there is only limited type-related compositional variation (Killops et al., 1998). The effects of oxygen-group suppression of the FID signal during Rock-Eval analysis does not appear to be able to account for all the observed initial increase in HI; structural rearrangements may exert the primary influence

* Corresponding author. Address: 3 The Fort Cawsand, Torpoint, Cornwall PL10 1PL, UK.

E-mail address: killops@macace.co.uk (S. Killops).

(Boreham, Horsfield, & Schenk, 1999; Boudou, Espitalié, Bimer, & Salbut, 1994; Killops, Allis, & Funnell, 1996; Killops et al., 1998). Jarvie and Lundell (2001) noted comparable behaviour for some Monterey Formation kerogens exhibiting high atomic O/C ratios, and the kerogens also exhibited kinetic similarities to low-maturity coals.

Structural rearrangements have important implications for the kinetic modelling of petroleum generation from coals (Boreham et al., 1999; Schenk & Horsfield, 1998), and are the subject of this article. Normally, source-rock samples on the verge of entering the oil window are selected for determining petroleum potential and kinetic parameters, but misleading transformation histories are likely if structural rearrangement continues into catagenesis, with the production of significant amounts of new bonds with different dissociation energies from those in the immature samples. One way to assess the efficacy of using immature samples to predict kerogen transformation is to compare the kinetic parameters derived from suites of naturally matured samples of similar kerogen type. Using this approach Schenk and Horsfield (1998) demonstrated that naturally matured Toarcian Posidonia shales (type II kerogen) produced HI transformation-rate ($\text{mgHC g C}_{\text{org}}^{-1} \text{ } ^\circ\text{C}^{-1}$) vs. temperature curves for typical geological heating rates such that the curve for a mature sample fell entirely beneath those of all the less mature curves (which are termed nested envelopes hereafter). This behaviour is to be expected if there is little, if any, production of new bonds with higher dissociation energies during natural maturation and suggests that immature samples can indeed be used to predict the kinetics of mature samples of this type of kerogen.

Corresponding studies on a suite of Westphalian vitrain coals from the Ruhr area produced different results. The higher maturity samples produced HI transformation-rate

curves that extended to progressively higher temperatures beyond the immature curves. In contrast, laboratory-matured coal samples produced transformation-rate envelopes that nested under those of the coals of lowest natural maturity, whether open- or closed-system pyrolysis was used for kinetic analyses (Schenk & Horsfield, 1998). These results led Schenk and Horsfield (1998) to conclude that various reactions occur during natural maturation, resulting in the formation of bonds with higher dissociation energies than originally present in the immature coals, that do not occur at the high heating rates used during artificial maturation whatever pyrolysis system is used. The unpredicted reaction pathways were mainly attributed to solid-state aromatisation of the macromolecular matrix, which compete with petroleum generation, particularly over the high- to medium-volatile bituminous rank range (VR \sim 0.6–1.5%).

The object of the present study is to investigate the maturity range over which the apparent structural rearrangement of the coal macromolecules occurs, with a view to determining whether there is an optimum sample maturity range for use in kinetic modelling of petroleum generation. A suite of 13 Late Cretaceous to Paleocene coals from Tara-1 well, Great South Basin, New Zealand, was selected for bulk-transformation kinetic studies. These coals, previously characterised by Killops, Cook, Sykes, and Boudou (1997), Killops et al. (1998) and Sykes et al. (1998), extend over a wide maturity range encompassing the onset of oil generation and expulsion, and exhibit compositional variations attributable predominantly to maturity variation. They have a relatively high hydrogen content, lying within the upper part of the New Zealand Coal Band (Fig. 1(a)). All the coals fall within the *Phyllocladidites mawsonii* (PM) assemblage, which is characterised by its dominant podocarp signature in pollen and biomarker distributions (Killops, Raine, Woolhouse, & Weston, 1995; Raine, 1984).

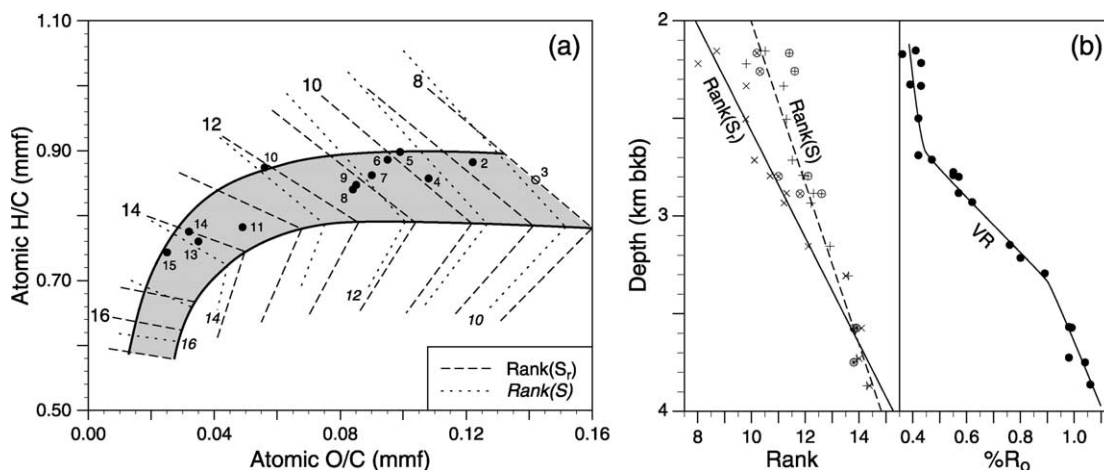


Fig. 1. (a) Van Krevelen diagram showing part of the New Zealand Coal Band, the relative positions of the Tara coals (sample numbers as in Table 1 and Rank(S) and Rank(S_r) isorank lines. (b) Depth trends for Tara coals of Rank(S_r) ($r = 0.96$) and Rank(S) ($r = 0.95$) derived from atomic H/C and O/C data (circled points are rank values obtained in 1978 from CV and VM data), and vitrinite reflectance.

The Late Cretaceous coals belong to the NZ Mata Series (Piripauan (85–81 Ma) and Haumurian (81–65 Ma) stages), and the Paleocene coals to the Teurian Stage of the Dannevirke Series (65–55 Ma).

2. Samples and methods

The samples used in this study were collected in 1995 from well cuttings held in the Gracefield Sample Library of the NZ Ministry of Economic Development (formerly Ministry of Commerce). The two shallowest samples (2 and 4) are of Paleocene age and the remaining 11 samples Late Cretaceous. The cuttings were washed to remove drilling mud and dried (50 °C). Coal fractions of spec. grav. ≤ 1.45 were isolated by flotation (sodium polytungstate solution), which corresponds to an ash content of $< 20\%$. After crushing to < 1 mm particles, small representative sub-samples were removed for petrographic analysis. The remaining material was crushed to a fine powder prior to the following analyses.

Proximate analysis (moisture, ash, volatile matter and fixed carbon), ultimate analysis (C, H, N and S measured, O by difference) and calorific value were undertaken by CRL Energy Ltd, New Zealand, following international and in-house standard procedures. Rock-Eval analyses were undertaken by IFP, France, using a Rock-Eval II instrument.

In the discussion of generation and expulsion of paraffinic oils from Tara-1 coals by Killops et al. (1998), the Rank(S) scale of Suggate (1959), adapted to the van Krevelen diagram (axes of atomic O/C and H/C; Fig. 1(a)) by Sykes, Suggate, and King (1992), was adopted as a maturity scale. Killops et al. (1998) and Sykes et al. (1998) assigned Rank(S) values to the onset of generation and expulsion of oil. Suggate (2000, 2002) has now presented a fully revised scale, termed Rank(S_r), in which rank increments are designed to represent more accurately unit increments of maximum temperature. Consequently a broadly uniform geothermal gradient results in an effectively linear increase in Rank(S_r) with depth. Two versions of the Rank(S) and Rank(S_r) scales are available: one based on a cross-plot of atomic O/C and H/C (both on the mineral matter-free basis) and the other, a cross-plot of calorific value and volatile matter (both on the dry, mineral matter- and sulphur-free basis). This paper uses the Rank(S_r) scale based on atomic O/C and H/C, although measured or estimated Rank(S) values are given where necessary for comparison with previous studies (see Fig. 1(b) for depth trends).

From comparison with a set of 7 Tara-1 coals analysed in 1978 during or shortly after drilling of the well (Hunt International Petroleum, 1978), it is clear that the coals in the present study had experienced significant oxidation in storage prior to the analysis of standard coal properties in 1995. The calorific values of samples 7 and 8, for example, show decreases of 440 and 410 Btu $1b^{-1}$ (1.02 and

0.95 MJ kg^{-1} ; dry, ash-free basis) between analysis in 1978 and 1995. Among basic coal properties the effects of coal oxidation are greatest on calorific value and oxygen content and accordingly, if oxidation is significant, these parameters need to be adjusted to obtain more reliable rank determinations. Because ultimate analyses were not undertaken on the 1978 samples direct comparison of oxygen contents with the 1995 samples cannot be made. Instead, adjustments to the oxygen contents of the 1995 samples have been made based on a study of two sets of coal samples from the Gironville drillhole in the Lorraine Basin, France (Appendix 2 of Suggate, 2000). The initial set was analysed shortly after the well was drilled and was reported in Alpern (1966) and the second set was analysed 20 years later and reported in Rouzaud, Geuchchati, Kister, and Conard (1991); the time lapse between the two sets of samples is similar to that of the two sets of Tara samples. The same rate of oxidation of the Gironville coals was assumed for the Tara coals and a proportional increase in oxygen (17/20 of that at Gironville) was applied to the 1995 sample set and Rank(S_r) values adjusted accordingly. The lowest rank Tara coals are lower rank than any at Gironville, requiring extrapolation from the Gironville data. Comparison of the adjusted Rank(S_r) and Rank(S) values with values recorded in the initial 1975 samples is discussed below.

Prior to kinetic analysis, all coal samples were subjected to solvent extraction followed by thermal-extraction at 250 °C in an attempt to remove bitumen and so minimise any influence it may have on subsequent kinetic pyrolyses. Volatile organics that vaporize during pyrolysis experiments behave as zero-order kinetic reactions. Depending upon the yield of volatiles, kinetic results can be adversely affected (Jarvie, 1991). Thermally flushing the sample at 250 °C remains the most effective means of removing volatile hydrocarbons up to $\sim C_{50}$, based on thermal-extraction high-temperature GC analysis.

Open-system pyrolysis was completed using the SR Analyzer (HISI Analytical Technologies). Pyrolysis data were acquired from 250 to 850 °C. Absolute temperature accuracy was ± 1 °C, and accurate temperature measurement was achieved by the uniform oven temperature of the instrument and by measuring the precise temperature at the sample. Five different heating rates were utilised between 1 and 30 °C with duplication of analyses at the slowest and fastest rates. The carrier gas, an often overlooked component of kinetic experiments, was helium, which exhibits the best conductivity of inert gases. Data were assembled into a file consisting of ~ 200 data points of time, true temperature, and rate (FID response) for input into the KINETICS2000 program.

Three optimisations were performed on each set of kinetic data, using the kinetics software: (1) discrete activation-energy (E_{act}) distribution with a single, variable frequency factor (A); (2) discrete- E_{act} distribution with a fixed A value ($10^{14} s^{-1}$); and (3) Gaussian- E_{act} distribution

with a single, variable A value. All reactions orders were set equal to 1.

An aliquot of sample 6 was artificially matured by hydrous pyrolysis. The extracted sample was loaded into a 71 ml Parr reactor, topped with twice its volume of water, and a head pressure of helium applied after the reactor was sealed. The reactor was heated isothermally at 350 °C for 24 h with the temperature being recorded every minute; temperature measurements were accurate to within ± 3 °C. The time and temperature conditions were chosen to achieve $\sim 50\%$ kerogen conversion, based on estimation from bulk kinetic data.

For the purposes of constructing a maturation model for Tara-1 well, there is effectively no difference between driller's depth and true vertical depth in Tara-1. Minimal deviation was recorded down to 3600 m below Kelly bushing (bkb), but between 3940 and 4330 m bkb deviation increases to 9° before declining to 4.5° at 4740 m bkb (Hunt International Petroleum, 1978). Consequently, there may be a 4.5 m discrepancy between the along-hole and true vertical depths. The depth of the base of the Piripauan stage (85 Ma, at ~ 4160 m below sea floor (bsf)) may be overestimated by 3.75 m and all units beneath by 4.5 m. This discrepancy is negligible compared with other potential errors in the numerical modelling, such as compaction parameters. Water depth (123.4 m relative to mean sea level) plays no part in the maturity modelling other than to constrain the temperature at the top of the sediment pile (hence depth bsf, 154.5 m less than depth bkb, is used in Fig. 10).

The thermal model for Tara-1 used a fairly hot, pre-sedimentation, steady-state crustal regime with a surface heat flow of 60 mW m⁻². The onset of crustal rifting and sedimentation occurred at ~ 100 Ma (Clarence stage), and rifting continued until 81 Ma (the end of the Piripauan stage) with an extension (β) factor of 1.7 (Cook et al., 1999). The basal lithospheric heat flow was modelled to increase from 40 to 55 mW m⁻² during rifting and then to decrease to 35 mW m⁻², which provided an excellent fit of modelled and measured VR and bottom-hole temperature data.

Kerogen maturation was modelled using a one-dimensional, finite-element code, BASSIM (Armstrong, Chapman, Funnell, Allis, & Kamp, 1996). Sediment thicknesses (after Cook et al., 1999) included 2 km of Raukumara and Clarence series (> 85 Ma) beneath the well bottom.

3. Results

Geochemical data on the bulk coals from Tara-1 have been reported previously (Killops et al., 1998) and are summarised, together with assigned rank values, in Fig. 2 and Table 1. The samples subjected to kinetic analysis (Table 1) were selected on the basis of there being adequate sample remaining from the set of samples for which Rock-Eval and elemental analysis data were available. The only exception is sample 16 (3958 m), of which insufficient material remained for an ultimate analysis; its rank values are derived from the downhole rank gradients in Fig. 1(b). The 13 samples span a moderately wide (oxygen-adjusted) Rank(S_r) range 8.7–15.1 (Rank(S) 10.5–14.7). It is clear from Fig. 1(b) that the adjustment of measured ranks for oxidation has yielded values close to those of the unoxidised coals of the 1978 set in the middle to high rank parts of the sequence, but greater adjustment is required for the lower rank samples, which appear to have been affected more by the oxidation. The set of samples subjected to kinetic analysis comprises a relatively restricted range of coal type, as judged by chemical and petrographic compositions. All of the samples lie within the upper half of the NZ Coal Band (Fig. 1(a)), which itself is representative of the progressive maturation of coals of relatively high hydrogen content. Accordingly, the Tara coals have notably higher hydrogen contents than Carboniferous coals from the northern hemisphere, and are typically vitrinite-rich ($> 80\%$ mmf) and poor in both inertinite and liptinite (each $< 10\%$).

Tara coal sample 2 contains a significant amount of migrated bitumen, on the basis of mature biomarkers distributions (Killops et al., 1998) and abundant short-chain n -alkanes, when compared with the underlying samples.

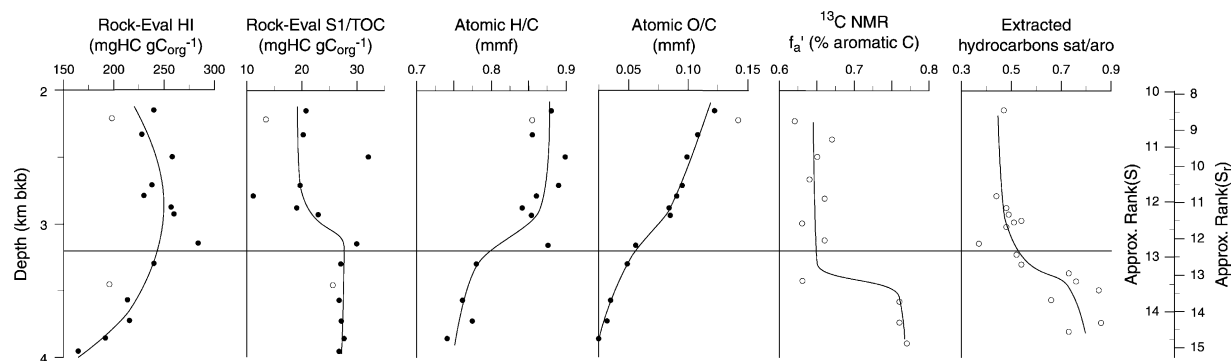


Fig. 2. Summary of geochemical data for bulk-coal samples from Tara-1 well. Solid points indicate samples for which kinetic data are discussed. Horizontal rule indicates approximate onset of significant paraffinic-oil expulsion (after Killops et al., 1998). Rock-Eval, elemental analysis and extracted bitumen data after Killops et al. (1998); ¹³C NMR data after Dickinson, Newman, and Collen (1991); atomic O/C data corrected for oxidation during storage (see Section 2). Rank(S) and Rank(S_r) depth scales derived from Fig. 2(b).

Table 1
Geochemical and kinetic data for Tara coals

Tara coal sample	2	4	5	6	7	8	9	10	11	13	14	15	16	6m
Mean depth (m bkb)	2156	2335	2504	2714	2794	2885	2934	3153	3304	3574	3729	3866	3958	2714
Depth range (ft bkb)	7060–90	7630–90	8200–30	8890–920	9160–75	9460–70	9610–40	10,330–60	10,810–70	11,710–40	12,220–50	12,670–700	12,970–13,000	8890–920
TOC (%) ^a	58.9	64.6	62.4	63.7	69.3	72.4	64.6	70.2	77.2	79.8	72.6	74.1	77.0	74.4
HI (mgHC g C _{org} ⁻¹)	242	230	260	240	232	259	262	286	242	216	218	194	167	106 ^b
T _{max} (°C)	415	420	423	429	433	433	433	437	442	451	451	453	457	n.d.
Ultimate C (%) ^c	59.1	64.6	63.3	64.4	69.0	71.1	63.4	70.4	77.6	80.0	72.6	75.7	n.d.	n.d.
S (%) ^c	6.0	4.4	4.1	3.1	0.9	1.4	1.3	0.9	1.0	0.7	0.7	0.7	n.d.	n.d.
Atomic H/C mmf	0.882	0.857	0.898	0.886	0.862	0.840	0.847	0.874	0.782	0.760	0.775	0.743	n.d.	n.d.
Atomic O/C mmf ^d	0.122	0.108	0.099	0.095	0.090	0.084	0.085	0.056	0.049	0.035	0.032	0.025	n.d.	n.d.
Rank(S)	10.5	11.2	11.3	11.5	11.9	12.3	12.2	12.9	13.6	13.9	13.9	14.3	14.7 ^e	n.d.
Rank(S _e)	8.7	9.8	9.8	10.1	10.7	11.3	11.2	12.1	13.5	14.1	14.0	14.4	15.1 ^e	n.d.
A (10 ¹⁴ s ⁻¹) ^f	7.1566	18.165	9.1538	4.0161	3.6064	0.73988	0.46727	4.5106	5.4620	9.6721	4.3276	2.9240	4.4433	0.40334
42 kcal mol ⁻¹ (%) ^f	0	0	0	0	0	0	0.15	0	0	0	0	0	0	0
43 kcal mol ⁻¹ (%) ^f	0	0	0	0	0	0	0.67	0	0	0	0	0	0	1.79
44 kcal mol ⁻¹ (%) ^f	0	0	0	0.02	0	0	0.24	0.27	0	0	0	0.23	0.03	0
45 kcal mol ⁻¹ (%) ^f	0	0	0	0.07	0	0	0.01	0.53	0	0	0	0.15	0.16	1.50
46 kcal mol ⁻¹ (%) ^f	0.04	0	0	0.01	0	0	0.32	0.41	0	0	0	0.34	0.06	2.15
47 kcal mol ⁻¹ (%) ^f	0.13	0	0.02	0.15	0	0	1.63	0.84	0	0	0.14	0.42	0.30	0.73
48 kcal mol ⁻¹ (%) ^f	0.26	0	0.18	0.17	0.09	0	0.33	0.67	0	0	0.22	0.57	0.18	3.30
49 kcal mol ⁻¹ (%) ^f	0.64	0.01	0.09	0.37	0.22	0	1.36	1.12	0.12	0.11	0.25	0.80	0.46	2.05
50 kcal mol ⁻¹ (%) ^f	0.60	0.55	0.43	0.40	0.27	0	1.16	0.85	0	0.13	0.49	0.91	0.44	15.44
51 kcal mol ⁻¹ (%) ^f	2.07	0.29	0.30	0.85	0.93	0	7.14	1.59	0.43	0.20	0.52	0.87	0.67	17.54
52 kcal mol ⁻¹ (%) ^f	3.19	1.06	0.92	1.14	0	7.57	30.12	0.84	0.37	0.45	0.85	1.39	0.63	8.17
53 kcal mol ⁻¹ (%) ^f	7.36	1.69	1.11	2.64	2.20	33.40	19.56	1.52	0	0.42	0.82	0.76	1.19	8.60
54 kcal mol ⁻¹ (%) ^f	10.28	2.72	4.78	8.85	5.09	16.54	15.77	2.66	0	0.94	0.83	1.86	0.74	6.79
55 kcal mol ⁻¹ (%) ^f	14.86	6.50	12.72	25.09	25.99	17.50	0	1.72	2.32	0.15	2.76	4.25	2.49	6.94
56 kcal mol ⁻¹ (%) ^f	15.12	14.22	22.95	19.26	19.67	4.09	0.89	25.94	17.35	1.95	11.26	12.48	6.30	2.70
57 kcal mol ⁻¹ (%) ^f	13.27	18.20	18.92	16.01	17.56	6.44	2.06	14.51	18.20	9.89	17.55	21.44	12.69	6.05
58 kcal mol ⁻¹ (%) ^f	9.35	15.63	12.54	7.27	6.75	1.65	3.29	11.96	18.81	16.55	20.03	16.73	19.27	0.64
59 kcal mol ⁻¹ (%) ^f	6.06	12.69	7.76	4.90	5.88	4.22	0.42	3.91	9.21	18.87	9.94	10.25	12.44	5.54
60 kcal mol ⁻¹ (%) ^f	4.16	7.16	4.32	2.43	2.13	0	2.19	5.51	9.47	12.03	10.06	6.49	11.08	0
61 kcal mol ⁻¹ (%) ^f	3.29	4.68	3.14	3.69	4.63	2.24	1.11	1.79	4.17	9.08	4.45	6.51	6.29	4.38
62 kcal mol ⁻¹ (%) ^f	1.98	3.27	2.64	0	0	2.10	0	2.96	6.89	7.50	6.81	1.93	7.82	0
63 kcal mol ⁻¹ (%) ^f	2.02	2.89	1.76	2.47	2.95	0	0	0.32	0	3.88	0	2.91	2.24	2.37
64 kcal mol ⁻¹ (%) ^f	0.79	1.26	0	1.17	1.64	0	2.59	2.35	4.68	5.55	4.96	3.42	3.60	1.20
65 kcal mol ⁻¹ (%) ^f	1.06	1.85	2.29	0	0	0	0	0	2.15	0	2.22	0	4.22	0
66 kcal mol ⁻¹ (%) ^f	1.32	0	0.048	0	0	4.26	0	0	0	4.74	0	0	0	0
67 kcal mol ⁻¹ (%) ^f	0	2.07	0	3.05	4.00	0	0	2.25	0	1.66	0	5.28	0	2.13
68 kcal mol ⁻¹ (%) ^f	0	0.46	0	0	0	0	0	0	5.84	0	5.84	0	6.71	0
69 kcal mol ⁻¹ (%) ^f	2.15	0	2.61	0	0	0	0	0	0	0	0	0	0	0
70 kcal mol ⁻¹ (%) ^f	0	0	0	0	0	0	0	0	0	5.91	0	0	0	0
71 kcal mol ⁻¹ (%) ^f	0	2.81	0	0	0	0	0	0	0	0	0	0	0	0
A (10 ¹⁴ s ⁻¹) ^g	9.1201	26.186	17.910	8.3636	8.4289	1.6761	26.748	5.1123	104.38	179.00	143.48	25.204	93.900	0.0256
E _{act} (kcal mol ⁻¹) ^g	56.425	58.226	57.764	57.061	57.43	55.18	58.811	56.698	62.386	63.893	63.446	61.027	63.497	51.567
SD (% E _{act}) ^g	5.0143	4.3031	3.7394	3.631	3.5804	3.2977	3.8815	3.8154	4.2193	4.5277	4.5383	4.4718	4.9862	7.129

^a Rock-Eval TOC.

^b Equivalent HI value.

^c Air-dried basis.

^d O adjusted for oxidation during storage.

^e Projected rank value from Fig. 1(b).

^f Data from discrete-E_{act}, free-A kinetic optimisation.

^g Data from Gaussian-E_{act}, free-A kinetic optimisation.

The variations in properties that commence at $\text{Rank}(S_r) \sim 12.5$ ($\text{Rank}(S) \sim 13$) in Fig. 2 are believed to be related to the onset of significant expulsion of saturates (predominantly *n*-alkanes). For example, there is a fairly abrupt decline in atomic H/C (see also Fig. 1(a)) and rise in aromatic-C content of the bulk coals, while extracted hydrocarbons exhibit an increase in saturates/aromatics (wt. basis). There are also compositional changes in biomarkers that are consistent with the onset of the main phase of oil expulsion (Killops et al., 1998).

The kinetic parameters obtained from a discrete- E_{act} distribution, free frequency factor, optimisation using KINETICS2000 are given in Table 1. A consequence of the single *A* value in discrete- E_{act} kinetic models is that *A* values, which can be considered a weighted average, tend to increase with maturity in naturally matured samples, up to ca. 1.7% R_r for coals (Jarvie, 1991; Schenk and Horsfield, 1998). However, the *A* values for the Tara coals do not appear to exhibit such a maturity trend.

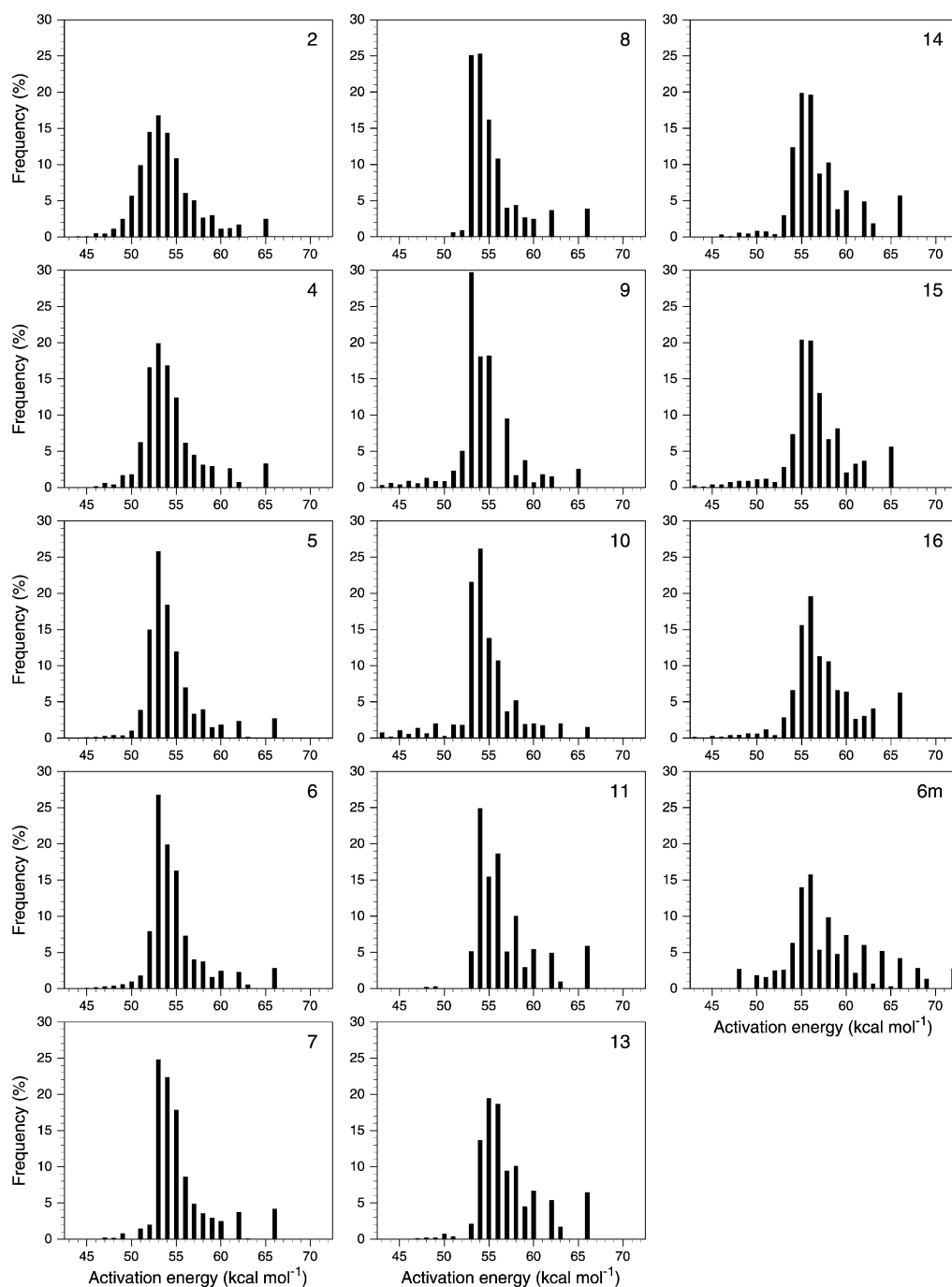


Fig. 3. Comparison of E_{act} distributions for Tara coals based on optimisation using discrete- E_{act} distribution with fixed frequency factor (10^{14} s^{-1}).

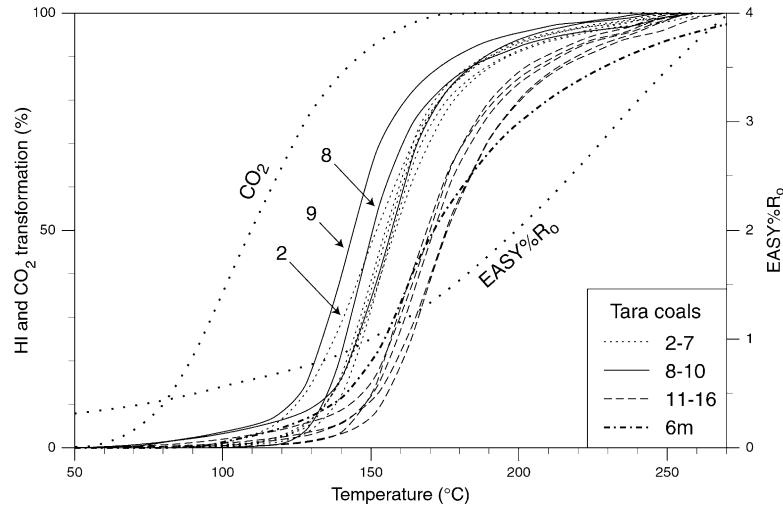


Fig. 4. HI transformation vs. temperature plots at a uniform heating rate of $3\text{ }^{\circ}\text{C my}^{-1}$ for extracted Tara coals using discrete- E_{act} distribution with free-A optimisation of open-system pyrolysis data. CO_2 generation kinetics after Burnham and Sweeney (1989) and EASY% R_o after Sweeney and Burnham (1990).

Kinetic optimisation for the Tara coals was also performed for a fixed frequency factor of 10^{14} s^{-1} , in order to facilitate comparison of discrete- E_{act} distributions, as shown in Fig. 3. With increasing burial depth and maturity the expected decline in low E_{act} values is observed. Not necessarily predicted is the rapid decline in relative abundance of 53 kcal mol^{-1} and increase of $> 60\text{ kcal mol}^{-1}$ between samples 10 and 13, and the significant contribution $\leq 50\text{ kcal mol}^{-1}$ in samples 9 and 10 that is not exhibited by vertically adjacent samples. The artificially matured sample 6m corresponds to 56% conversion on the basis of measured HI, which compares favourably with the 54% conversion

predicted by the free-A discrete- E_{act} distribution kinetic optimisation for the original sample 6. The inaccuracies inherent in fitting E_{act} distributions to the same A value are reflected in the large relative abundance of a single E_{act} at $\geq 65\text{ kcal mol}^{-1}$; the problem appears more acute for 6m. The free-A discrete- E_{act} optimisation is not without problems of this kind (Table 1). In addition, even slight compositional changes related to kerogen-type variation may affect the kinetic data.

HI transformation curves at a uniform heating rate of $3\text{ }^{\circ}\text{C my}^{-1}$ obtained from the discrete- E_{act} free-A optimisation are shown in Fig. 4. This heating rate is geologically meaningful, and the burial/thermal history model for Tara-1

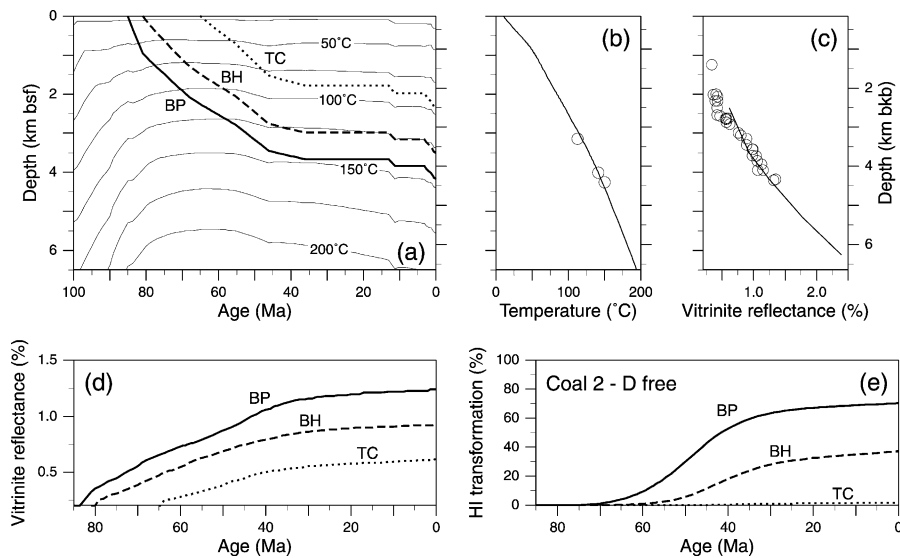


Fig. 5. Thermal and kinetic modelling for Tara-1 well, Great South Basin, New Zealand. Thermal model (a) is constrained by present-day surface heat flow of 61 mW m^{-2} and measured bottom-hole temperatures (b) and vitrinite reflectance (c). Vitrinite reflectance (d) is modelled using EASY% R_o (after Sweeney & Burnham, 1990) and kerogen transformation (e) is modelled using discrete- E_{act} free-A data for coal sample 2. Tracked Cretaceous intervals: TC = top Cretaceous (65 Ma), present depth 2350 m bsf; BH = base Haumurian (81 Ma), present depth 3500 m bsf; BP = base Piripauan (85 Ma), present depth 4160 m bsf.

(Fig. 5) suggests the Tara coals experienced a similar heating rate from 85 to 45 Ma. The naturally matured coals can be divided into three groups. The first includes the least mature samples 2–7. As might be expected, HI transformation for sample 2 is more advanced at low temperatures than for the other samples in this group, but samples 5–7 exhibit similar transformation curves. The high maturity group, samples 11–16, have similar HI transformation curves in Fig. 4, reflecting the higher temperatures needed for the onset of significant HI transformation in these samples compared with the least mature group. The group of three intermediate-maturity samples 8–10 exhibit anomalous HI transformation curves which do not lie between the low and high maturity groups and involve retrogression. The curve for sample 8 is shifted to lower temperature, approaching that of sample 2, which is a consequence of the narrow E_{act} range with dominant contribution from 53 kcal mol^{-1} (Table 1). The curve for sample 9 is shifted to even lower temperature, which is the result of the dominant contribution from 52 kcal mol^{-1} (Table 1). The curve for sample 10 shows a return towards the expected transition from low to high maturity groups, being similar to the those for samples 5–7. However, like sample 9, it exhibits significant transformation of HI at relatively low temperatures (even greater than for sample 2), which can be attributed to the significant relative abundance of low E_{act} values in Table 1.

Comparison of kinetics for the free-A, discrete- E_{act} distribution optimisation can be achieved by plotting the rate of HI transformation per °C vs. temperature at a uniform heating rate and adjusting for the effects of carbon loss on HI with increasing maturity in a series of related samples (Schenk and Horsfield, 1998). The C-loss adjusted HI values (hereafter referred to as normalised HI) relate the remaining hydrocarbon potential to the initial 1 g of C in the lowest maturity sample rather than to the ever decreasing amount of C left in more mature samples that results from the loss of C-containing compounds. When corrected for C losses the transformation envelopes for a particular sample should lie

under those of all less mature samples, assuming that each coal sample started off with the same composition at the beginning of catagenesis so that initial HI is constant and maturity is the only variable. The transformation-rate envelopes should form a nested set. Meaningful correction for the loss of C up to a Rank(S_r) of ~ 11 (samples 2–8) is difficult because of the combined effects of O-group suppression of the FID signal during Rock-Eval analysis and structural rearrangements (Boudou et al., 1994; Killops et al., 1996). In addition, C loss after the onset of significant oil generation in naturally matured samples can only be estimated (Schenk & Horsfield, 1998). Consequently, a degree of error in normalising transformation-rate envelopes is inevitable.

In Fig. 6 the HI transformation-rate envelope are shown for the discrete- E_{act} free-A kinetic optimisation data for a geologically meaningful heating rate of 3 °C my^{-1} for measured HI values (i.e. without any attempt at correction for increasing C losses from the more mature samples). The three main groups of samples, as described above, are highlighted in turn in the three plots. Because correction for C loss causes the normalised HI transformation-rate to be lower than the measured rate, if the uncorrected transformation curves for successively more mature samples always lie under those of lower maturity samples it can be concluded that the corrected curves would do likewise. However, the three groups of transformation-rate envelopes do not nest. Firstly, a significant proportion of the envelope for each of the high-maturity group of coals lies on the high-temperature side of the low-maturity group of samples. Secondly, a large proportion of the envelopes for samples 8 and 9 lies on the low-temperature side of the low-maturity group of samples (and the relatively high transformation rates for samples 9 and 10 at low temperatures can also be observed). Thirdly, although the transformation-rate envelope for the artificially matured sample 6m nests under the curves of the low-maturity group, it does not encompass the high-maturity group curves.

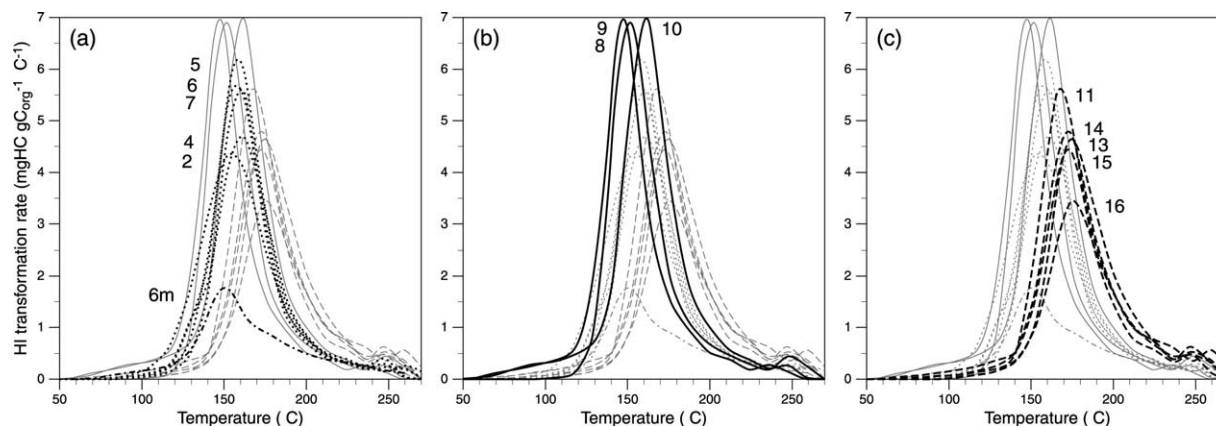


Fig. 6. HI transformation-rate vs. temperature plots (at a uniform heating rate of 3 °C my^{-1}) for extracted, naturally matured, Tara coals and the artificially matured sample 6m, using measured HI values and kinetic-parameter optimisation based on discrete- E_{act} distribution with single, variable frequency factor. Three groups can be distinguished on the basis of nesting of transformation envelopes, corresponding to relative maturity: (a) low, (b) intermediate and (c) high.

Estimated correction for C loss is clearly required for adequate evaluation of the transformation-rate envelopes. In deriving the necessary corrections an assumption has to be made about the initial normalised HI. In Fig. 7(a) an idealised plot is shown of the depth trend of HI for the Tara suite of coals, labelled ‘corrected’, together with the associated suppression of the HI signal that would be required to produce the observed HI trend. For the least mature sample (sample 2) the corrected HI is $290 \text{ mgHC g C}_{\text{org}}^{-1}$, and the values extrapolated for the other samples are given in Table 2. By assuming C losses are mostly from hydrocarbon generation, to a first approximation, the fractional C loss $(1 - c_i)$ is given by $0.83(\text{HI}_i - \text{HI}_0)/(0.83\text{HI}_i - 1000)$, where HI_0 is the initial HI and HI_i is the HI of a more mature sample. The normalised HI is then $(\text{HI}_i)(c_i)$, as shown in Table 2, and the resulting plot of normalised HI vs. depth is shown by the trend labelled ‘HI’ in Fig. 7(b). The corresponding HI transformation-rate envelopes in Fig. 8(a) again do not nest uniformly.

Another way to estimate C loss is to apply the HI transformation kinetics for sample 2 to the modelled thermal histories of all the coals (Fig. 5), assuming an initial HI of $290 \text{ mgHC g C}_{\text{org}}^{-1}$ again, which corresponds to 24.1% of total C content. An additional correction can be made for loss of C-containing gases: on a CHO basis at Rank(S_r) ~ 8 , NZ coals typically contain $\sim 80\%$ C, $\sim 4\%$ O in carboxyl groups and $\sim 1.5\%$ O in carbonyl groups. The carboxyl-C corresponds to $\sim 1.9\%$ of total C and the carbonyl-C to $\sim 1.4\%$, i.e. $\sim 3.3\%$ of total C can potentially be lost as oxygen-containing gases that do not contribute to the S2 signal during Rock-Eval analysis. The loss of this C can be approximated by applying the published kinetics for CO_2 generation (Burnham & Sweeney, 1989) to the thermal history model of the Tara coals. It has a relatively small effect compared with the C loss corresponding to

the Rock-Eval S2 measurement. The resulting depth trend in apparent HI (i.e. where C loss from kerogen is taken into account) is shown in Fig. 7(a), and the normalised HI (i.e. related to the initial C content of sample 2) is shown in Fig. 7(b) and recorded in Table 2. The kinetic trend is similar to that obtained by the simple correction based only upon HI values, so the corresponding HI transformation-rate envelopes are not reproduced here.

Forcing all transformation-rate envelopes to nest uniformly produces the plots in Fig. 8(b). The corresponding correction factors that have to be applied to the observed HI values and the normalised HI values that result are given in Table 2. The HI datum for the nesting corrections was chosen as the maximum in the best-fit line for the measured HI, which occurs near sample 7. The measured HI values of more mature (deeper) samples were reduced and the measured HI values of less mature (shallower) samples were increased to achieve nesting of the transformation-rate envelopes. The chief reason for selecting this datum rather than the least mature sample is that the degree of possible HI suppression is greatest for the least mature samples and cannot be predicted accurately.

Similar comparisons of the transformation-rate envelopes from the discrete- E_{act} fixed-A and Gaussian- E_{act} free-A kinetic optimisations were also performed. The Gaussian kinetic data are given in Table 1 and the discrete- E_{act} distributions are shown in Fig. 3 for $A = 10^{14} \text{ s}^{-1}$. The envelopes for measured HI values are shown in Fig. 9(a) and (c) and the corresponding envelopes for normalised HI values (based on the HI trend in Fig. 7(b)) are shown in Fig. 9(b) and (d). The discrete- E_{act} fixed-A envelopes can be forced to nest without such a large decrease in HI between samples 7 and 11 as needed for the discrete- E_{act} free-A data, but the Gaussian data cannot be forced to nest without virtually all HI transformation occurring by sample 11 (Fig. 7(b)), which is unrealistic given the measured HI and

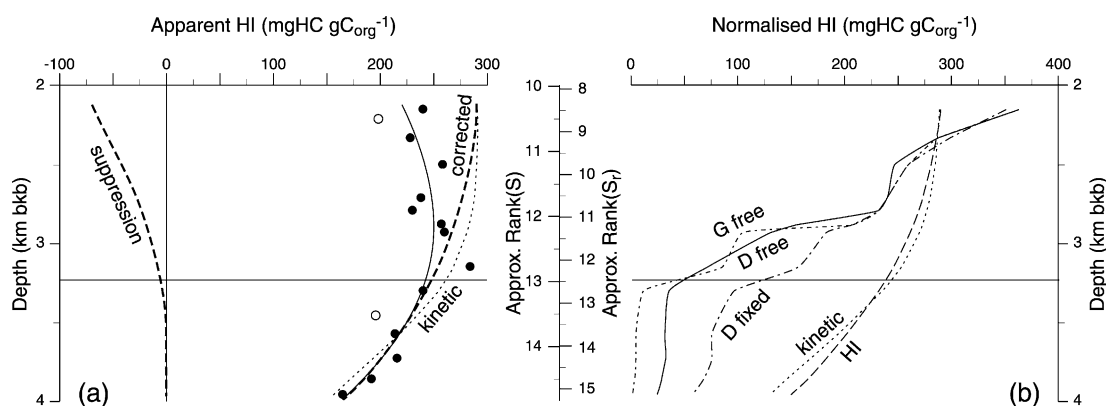


Fig. 7. (a) Possible suppression of HI and related correction as an explanation for observed trend (after Killops et al., 1998), together with HI predicted from Tara coal 2 kinetics, assuming initial HI of $290 \text{ mgHC g C}_{\text{org}}^{-1}$ and adjusting to apparent HI by correcting for C loss using HI transformation kinetics for Tara coal 2 and CO_2 generation kinetics (Burnham & Sweeney, 1989); (b) Various methods for normalising HI values: HI trend = corrected HI trends in (a) (with HI of $290 \text{ mgHC g C}_{\text{org}}^{-1}$ for Tara coal 2) adjusted for C loss using HI change; kinetic trend = variation predicted by HI transformation kinetics for Tara coal 2, assuming initial HI of $290 \text{ mgHC g C}_{\text{org}}^{-1}$; D free trend = HI values derived from nesting transformation-rate envelopes from discrete free-A optimisation in Fig. 8; D fixed trend = HI from nesting envelopes derived from discrete fixed-A optimisation in Fig. 9(b); G free trend = HI from closest approach to nesting of envelopes derived from Gaussian free-A optimisation in Fig. 9(d). See Table 2 for HI correction factors.

Table 2
HI correction data for comparison of transformation-rate curves

Tara coal	Observed ^a HI (mg g C ⁻¹)	Fit ^b HI (mg g C ⁻¹)	HI corrected ^c			Kinetics ^d				Discrete free-A nest ^e			Discrete fixed-A nest ^f			Gaussian free-A nest ^g		
			HI (mg g C ⁻¹)	C (%)	Norm HI (mg g C ⁻¹)	Trans HI _{kin} (%)	Trans C _{CO2} (%)	Norm HI (mg g C ⁻¹)	App HI (mg g C ⁻¹)	HI factor	Norm HI (mg g C ⁻¹)	Norm C loss (%)	HI factor	Norm HI (mg g C ⁻¹)	Norm C loss (%)	HI factor	Norm HI (mg g C ⁻¹)	Norm C loss (%)
2	242	222	290	100	290	0	25	290	291	1.50	363	-25	1.45	351	-21	1.50	363	-25
4	230	235	287	100	286	1	34	287	291	1.25	288	0	1.30	299	-4	1.25	288	0
5	260	240	283	99	281	2	46	285	290	0.95	247	13	1.00	260	8	1.00	260	8
6	240	247	277	99	273	3	55	280	288	1.00	240	13	1.00	240	13	1.00	240	13
7	232	249	273	98	268	4	60	277	286	1.00	232	15	1.00	232	15	1.00	232	15
8	259	250	269	98	263	6	65	273	283	0.60	155	42	0.80	207	23	0.80	207	23
9	262	250	267	98	260	7	68	270	281	0.50	131	51	0.70	183	31	0.40	105	61
10	286	245	254	96	244	13	76	253	268	0.25	72	72	0.55	157	38	0.30	86	66
11	242	242	249	96	238	19	81	235	254	0.15	36	86	0.40	97	61	<0.05	<10	>95
13	216	223	218	93	202	33	88	194	218	0.15	32	85	0.35	76	65	<0.05	<10	>95
14	218	207	201	91	183	42	91	168	193	0.15	33	84	0.35	76	62	<0.05	<10	>95
15	194	188	184	90	165	50	94	145	171	0.15	29	84	0.35	68	63	<0.05	<10	>95
16	167	173	170	88	150	55	95	130	156	0.15	25	85	0.35	58	66	<0.05	<10	>95
6m	106	109	122	84	103					0.05	5	96	0.40	42	66	<0.05	<10	>95

^a Measured HI.

^b HI corrected to best-fit curve (Fig. 7(a)).

^c HI from corrected curve (Fig. 7(a)), related C loss $([0.83(HI_i - 290)]/[0.83(HI_i) - 1000])$ and normalised HI (to 1 g of initial C).

^d HI transformation from discrete- E_{act} free-A kinetics for coal 2, CO₂ transformation from published kinetics (Burnham & Sweeney, 1989), normalised HI based on initial HI of 290 mgHC g C_{org}⁻¹ and coal 2 kinetics, apparent HI derived from normalised HI corrected for C loss using HI and CO₂ transformation kinetics (100% C_{HI} = 0.241 g, 100% C_{CO2} = 0.033 g).

^e Correction to observed HI values to achieve nested transformation-rate envelopes from discrete- E_{act} , free-A kinetic optimisation (Fig. 8(b)), and related C loss by comparison with corrected HI values in Fig. 7(a).

^f Correction to observed HI values to achieve nested transformation-rate envelopes from discrete- E_{act} , fixed-A kinetic optimisation, and related C loss by comparison with corrected HI values in Fig. 7(a).

^g Correction to observed HI values to achieve closest approach to nested transformation-rate envelopes from Gaussian- E_{act} , free-A kinetic optimisation, and related C loss by comparison with correction HI values in Fig. 7(a).

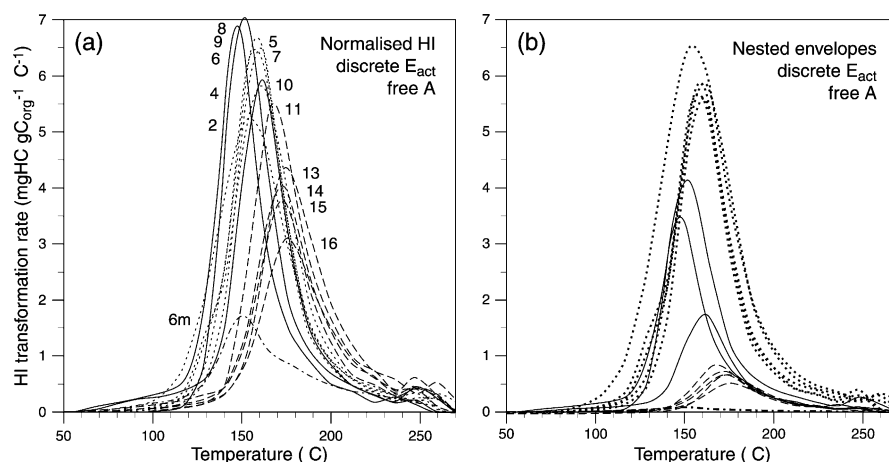


Fig. 8. HI transformation-rate vs. temperature plots (at a uniform heating rate of $3\text{ }^{\circ}\text{C my}^{-1}$) for extracted, naturally matured, Tara coals and the artificially matured sample 6 m using kinetic-parameter optimisation based on discrete- E_{act} distribution with single, variable frequency factor. (a) HI based on initial value of $290\text{ mgHC g C}_{\text{org}}^{-1}$ and following HI-depth trend in Fig. 7(b), normalised for C loss using HI values; (b) HI values adjusted for approximate nesting of transformation-rate envelopes (D free trend, Fig. 7(b)). HI correction data as in Table 2.

VR values of the more deeply buried samples. The HI corrections necessary for nesting are given in Table 2, together with the estimates of normalised C loss that would be required for the nested normalised HI values to yield

measured values equivalent to the corrected HI trend in Fig. 7(a).

Samples 8–10 clearly put severe constraints on the normalised HI values for the high-maturity group of coals to

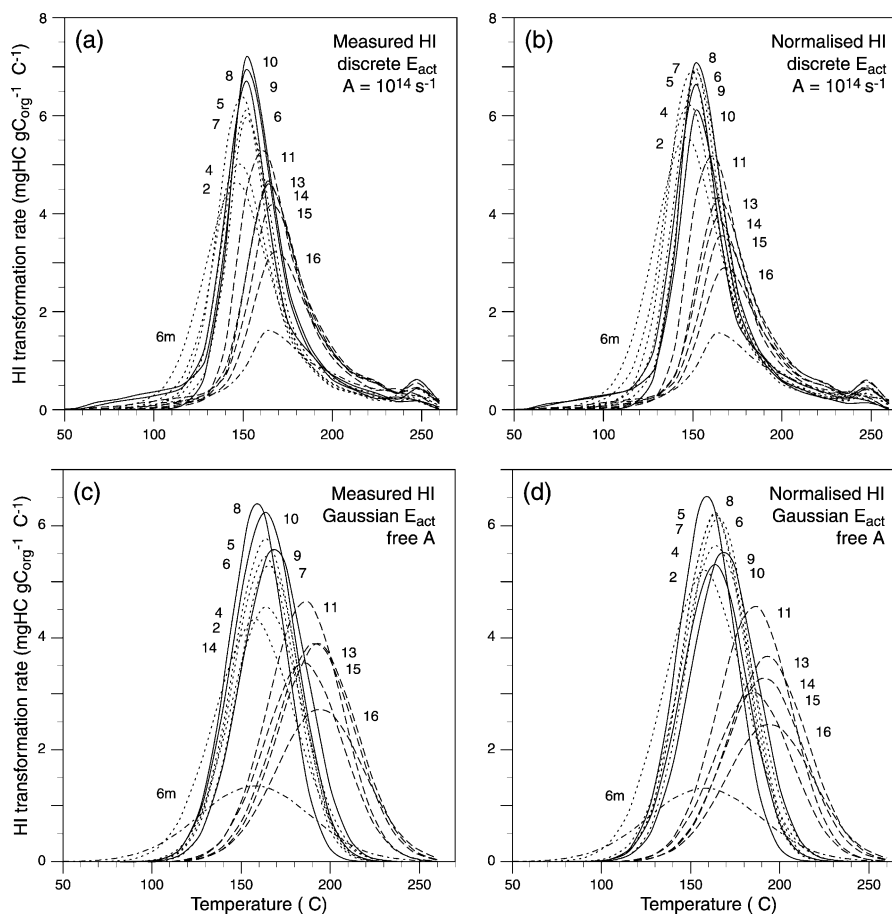


Fig. 9. HI transformation-rate vs. temperature plots (at a uniform heating rate of $3\text{ }^{\circ}\text{C my}^{-1}$) for extracted, naturally matured, Tara coals and artificially matured sample 6m. Kinetic optimisation parameters were: discrete- E_{act} distribution with fixed A value of 10^{14} s^{-1} (a,b); Gaussian- E_{act} distribution with single, variable A value (c,d). Plots are shown for measured HI (a,c) and normalised HI (b,d) values; the latter based on initial $290\text{ mgHC g C}_{\text{org}}^{-1}$ for Tara coal 2 and following HI trend in Fig. 7(b), which uses HI values to correct for C loss (see Table 2).

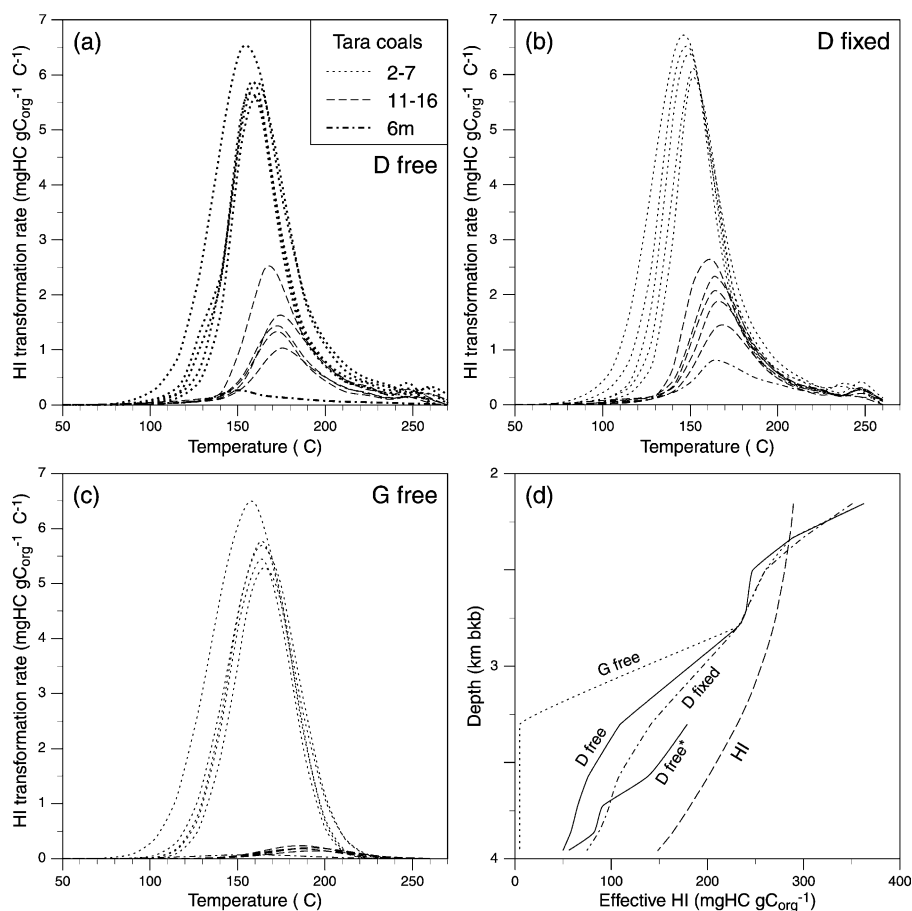


Fig. 10. Nesting of HI transformation-rate envelopes (at a uniform heating rate of $3\text{ }^{\circ}\text{C}\text{ m}^{-1}$) for extracted, naturally matured, Tara coals and the artificially matured sample 6m, but excluding samples 8–10. Kinetic optimisation parameters were: (a) discrete- E_{act} free-A; (b) discrete- E_{act} fixed-A (10^{14} s^{-1}); (c) Gaussian- E_{act} free-A; (d) normalised HI depth trends derived from (a)–(c) together with normalised HI trend from Fig. 7(b) (labelled HI) and the trend for discrete- E_{act} free-A if only coals 2 and 11–16 are nested (D free*, using same HI value of $363\text{ mgH g C}_{\text{org}}^{-1}$ for coal 2 as in D free trend). See Table 3 for HI adjustment factors.

Table 3

HI correction data for partial nesting of transformation-rate envelopes (excluding coals 8–10). See Fig. 10 for nested envelopes. All HI values are effectively normalised

Tara coal	Discrete free-A nest ^a			Discrete free-A nest ^b			Gaussian free-A nest ^c		
	HI factor	Norm HI (mg g C^{-1})	Norm C loss (%)	HI factor	Norm HI (mg g C^{-1})	Norm C loss (%)	HI factor	Norm HI (mg g C^{-1})	Norm C loss (%)
2	1.50	363	–25	1.45	351	–21	1.50	363	–25
4	1.25	288	0	1.30	299	–4	1.25	288	0
5	0.95	247	13	1.00	260	8	1.00	260	8
6	1.00	240	13	1.00	240	13	1.00	240	13
7	1.00	232	15	1.00	232	15	1.00	232	15
11	0.45	109	56	0.50	141	43	<0.05	<10	>95
13	0.35	76	65	0.50	108	50	<0.05	<10	>95
14	0.30	65	68	0.45	98	51	<0.05	<10	>95
15	0.30	58	68	0.45	87	53	<0.05	<10	>95
16	0.30	50	71	0.45	75	56	<0.05	<10	>95
6m	0.15	16	87	0.50	53	57	<0.05	<10	>95

^a Correction to observed HI values (Fig. 6) to achieve nested transformation-rate envelopes from discrete- E_{act} , free-A kinetic optimisation, and related C loss by comparison with corrected HI values in Fig. 7(a).

^b Correction to observed HI values (Fig. 9(a)) to achieve nested transformation-rate envelopes from discrete- E_{act} , fixed-A kinetic optimisation, and related C loss by comparison with corrected HI values in Fig. 7(a).

^c Correction to observed HI values (Fig. 9(c)) to achieve closed approach to nested transformation-rate envelopes from Gaussian- E_{act} , free-A kinetic optimisation, and related C loss by comparison with corrected HI values in Fig. 7(a).

achieve nesting of transformation-rate envelopes. Omitting coals 8–10 yields the nesting of transformation-rate envelopes shown in Fig. 10(a)–(c) for the three kinetic optimisation methods. The corresponding depth trends in normalised HI are shown in Fig. 10(d) and the adjustments to measured HI and resulting normalised C loss are given in Table 3. Again, the Gaussian- E_{act} free-A cannot be forced to nest without virtual elimination of HI potential for the high-maturity group of coals (samples 11–16; Fig. 10(c)). The rate of decrease in HI with depth is more reasonable for the two discrete- E_{act} models, although the projected C loss is still quite high (some 30–40% between samples 7 and 11) for a Rank(S_r) change of only ~ 3 . A further trend in Fig. 10(d), D free*, shows the effect of only considering the nesting of samples 11–16 under the transformation-rate envelope of sample 2, using the same HI value for coal 2 (363 mgHC g C_{org}⁻¹) as in the D free trend. Although the required HI (and total C) loss is lower than for the D free trend, it is still much higher than indicated by the observed HI values.

The implications for maturity modelling of the variations in recorded kinetic parameters can be examined using a thermal model for Tara-1 well. The dramatic rise of the modelled isotherms during the early part of the thermal history plot in Fig. 5(a) is due to the rifting and the thermal blanketing effect of the early sediments, resulting in early maturation of Cretaceous sediments. The good fit of modelled temperatures and VR values to measured values is shown in Fig. 5(b) and (c), respectively. Three Late Cretaceous (Mata Series) horizons are tracked, corresponding to the top and bottom of the Haumurian and Piripauan stages. Predicted VR and HI transformation plots are shown, respectively, in Fig. 5(d) based on EASY% R_o (Sweeney & Burnham, 1990) and Fig. 5(e) based on the discrete- E_{act} , free-A kinetics for coal 2.

4. Discussion

The discrete- E_{act} , free-A optimisation of bulk HI transformation kinetic data should provide a more realistic approach than either of the other two optimisation techniques, even bearing in mind the potential inadequacies of representing the transformation as a set of first order reactions sharing the same frequency factor. A Gaussian E_{act} distribution is unlikely to represent accurately the distribution resulting from the many different types of bonds present in coals inherited from epicuticular waxes, cutan/suberan, cutin, lignin, etc. (c.f. isolated-maceral kinetics in Michelsen & Khorasani, 1995). The fixed-A, discrete- E_{act} model does not permit the anticipated increase in A with increasing maturity (Jarvie, 1991).

Unreasonable constraints are placed on the trends in HI transformation and associated C loss in order to give full nesting of transformation-rate envelopes for the discrete- E_{act} free-A data derived from Fig. 8(b). For example, HI

transformation would have to occur over a narrow rank range and would be virtually complete by Rank(S_r) 12.5 (D free trend, Fig. 7(b)), C loss would be around 85% in the most mature samples and a loss of some 70% of C would occur between samples 7 and 11, all of which are unrealistic over the rank range involved. The main problem with forcing complete nesting of transformation-rate curves is the apparent shift to lower-energy bonds in samples 8 and 9, and to a lesser extent in sample 10 (Fig. 6). The S content of samples 8 and 9, although low, is a little higher than for the immediately stratigraphically adjacent samples, but not as high as for the least mature samples (Table 1). Consequently, it does not appear that S-bound organic material could account for the scale of the shift in transformation curve to lower temperature observed in Fig. 4. Nor do the slight type-related variation in composition of the coals and relatively minor effects of oxidation during storage appear likely to account for the abrupt and significant change in transformation-rate envelopes between samples 7 and 11, given the similarities within each of the low- and high-maturity groups of coals (Fig. 6). Another reason must exist for the unexpected behaviour of samples 8–10.

Overall, it does not appear possible to achieve nesting of transformation envelopes with sensible HI transformation or C-loss trends using the discrete- E_{act} free-A kinetic optimisation. In addition, it is impossible to achieve nesting of the artificially matured sample 6m under the transformation envelopes of the coals representing the highest natural maturity without an unreasonably high degree of HI transformation (Table 2). As noted above, the Gaussian- E_{act} free-A envelopes cannot be nested with any degree of reasonable HI decrease and related C loss (Table 2). The discrete- E_{act} fixed-A kinetic optimisation provides the least unreasonable HI vs. depth trend among the three sets of kinetic optimisations in Fig. 7(b), but again HI transformation occurs over a very narrow rank range and the corresponding C losses are still very high (some 40% of C still has to be lost between samples 7 and 11; Table 2). The inference from the transformation-envelope nesting studies, particularly the fact that artificial maturation of the Tara coal 6m does not mimic natural maturation, appears to support the contention that coal undergoes structural rearrangement during natural maturation (Schenk & Horsfield, 1998).

The maturity range over which structural rearrangement occurs is of importance in determining the maturity range over which the kinetics obtained from immature coals are applicable to the modelling of coal maturation. From the nesting studies it appears that the greatest adjustments occur over a relatively narrow maturity range of Rank(S_r) 10.5–13.5 (Fig. 7(b)). This can also be seen in the unadjusted transformation-rate curves in Figs. 6 and 9(a) and (c). There is no clear progression of the high-temperature limb of the envelopes to higher temperature for any of the three kinetic-optimisation methods; samples 4–7 form one tight grouping and 11–16 form another (Figs. 6 and 9). Only for

the discrete- E_{act} fixed-A optimisation is there any indication that samples 8–10 may represent a progression between the low- and high-maturity groups of coals (Fig. 9(a)). For the discrete- E_{act} free-A optimisation there is a definite jump in transformation curves in the range Rank(S_r) 10.5–13.5 (Rank(S) \sim 11.5–13.5). A similar jump in transformation-rate envelopes from open-system pyrolysis has been reported for a set of solvent-extracted, naturally matured, Carboniferous coals from the Ruhr area (Schenk & Horsfield, 1998). Above 0.92% R_r , all transformation envelopes nested under the 0.92% curve, and only for the one lower maturity sample (0.74% R_r) did the high-temperature limb shift to lower temperature (Fig. 5 of Schenk & Horsfield, 1998). The Rank(S_r) range over which this occurs is approximately the same as that observed in the Tara coals.

If the apparently aberrant samples 8–10 are omitted from the forced nesting of transformation-rate envelopes of the Tara coals, less extreme HI (and hence C losses) are required for the discrete- E_{act} optimisations, but the Gaussian- E_{act} optimisation still fails to provide nesting without the unrealistic virtual exhaustion of HI potential for samples 11–16 (Fig. 10). However, the C loss needed to give the corrected measured HI values for the discrete- E_{act} optimisations is still higher than can be reasonably expected (30–40% C loss between 7 and 11, Table 3). Even if nesting of only the high-maturity set of coals, 11–16, with coal 2 is considered, the required loss of C to yield the observed HI values would still be too high (see D free* trend in Fig. 10(d)).

The shift to higher temperature in the high-temperature limb of the transformation curves between the low- and high-maturity groups of coals is consistent with the appearance of new bonds with greater dissociation energies. Schenk and Horsfield (1998) attributed such behaviour to certain reactions that occur during natural maturation but which either do not occur or only occur to a partial extent under the higher-temperature and shorter-time conditions employed in laboratory pyrolysis.

Rogers, Suggate, Elphick, and Ross (1962) demonstrated that increasing the temperature of hydrous pyrolysis of a low-rank lignite resulted in increasing deviation from the NZ Coal Band on the volatile matter (VM) vs. calorific value (CV) plot in Fig. 11 (a similar deviation is also found using an atomic H/C vs. O/C plot). For a given CV value, the VM value is lower than expected for the NZ Coal Band. However, with increasing time at a particular pyrolysis temperature a path parallel to but at lower VM content than the NZ Coal Band is followed. This behaviour is consistent with the suggested importance of heating rate on the extent of structural rearrangement. Related behaviour has been noted for coals influenced by igneous intrusions (Francis, 1952; Rogers et al., 1962; Schopf & Long, 1966) but, unfortunately, articles in which the effects of the distance of a low-ash coal from a single igneous body on proximate and/or ultimate analytical data are rare. Data for low-ash

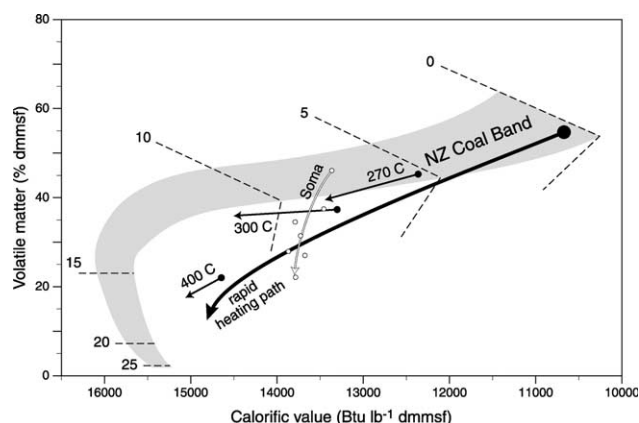


Fig. 11. Effects of heating rate on maturation path for Waimatua lignite in relation to NZ Coal Band (data after Rogers et al., 1962). Small solid arrows show isothermal evolution paths for lignite samples after hydrous pyrolysis at indicated temperatures; large solid arrow shows extrapolated path of rapid heating (Rogers et al., 1962). Outlined arrow shows effect of igneous intrusion on coals from Soma, Turkey (data for raw coals of k1 seam, air-dried basis only; after Karayigit & Whateley, 1997). Broken lines represent isoRank(S_r) lines (after Suggate, 2000); dmmf = dry, mineral-matter and sulphur free.

(< 20%, air-dried basis) coals from the k1 seam in the Soma Basin Turkey (Karayigit & Whateley, 1997) are plotted in Fig. 11. Although the data do not fit the idealised trend for rapid heating precisely, they do follow a similar trend of decreasing VM content with increasing temperature. Heating rate is clearly a key factor in the structural evolution of coals, leading to the lower extent of aromatisation in artificially matured coals, the differences in bulk-transformation kinetic parameters between naturally and artificially matured coals, and the lower hydrocarbon potentials reported for artificially matured coals compared with naturally matured samples of equivalent rank (Schenk & Horsfield, 1998).

The approximate proportion of HI attributable to apparently new, higher-energy bonds can be calculated from the area of the part of the transformation-rate envelope for Tara coal 11 that lies outside the high-temperature limb of the envelope of sample 7 in Fig. 8(a). The proportion of higher bond-energy components in sample 11 corresponds to \sim 20% of the HI value of sample 11 (or \sim 50 mgHC g C_{org}^{-1}).

Schenk and Horsfield (1998) suggested that potential candidates for the structural rearrangements are solid-state aromatisation reactions, which are likely to have their greatest influence on volatiles generation up to the boundary between medium- and low-volatile bituminous rank (VR \sim 1.3%, Rank(S_r) and Rank(S) \sim 15). Residual bitumen may take part in these aromatisation reactions; it begins to degrade thermally and to repolymerise at the upper end of the high-volatile bituminous A rank (Schenk & Horsfield, 1998). If the proposed solid-state aromatisation is a progressive reaction a sudden jump to higher temperature in the transformation envelopes would not be expected.

The fact that this jump coincides with the proposed onset of significant expulsion of paraffinic oil from the Tara coals (Killops et al., 1998) suggests that the presence of adsorbed bitumen plays a role, offsetting the effects of increasing solid-state aromatisation on the bulk-kinetic parameters prior to the main phase of oil expulsion. For the five post-expulsion samples of $\text{Rank}(S_r) > 13.5$ ($\text{Rank}(S) \geq 13.5$) any further structural rearrangements do not appear to affect the transformation envelopes to any great extent, which could reflect the important role of retained bitumen during structural rearrangement (Schenk & Horsfield, 1998).

As noted in Section 1, the increase in measured HI that occurs as maturity increases up to $\text{Rank}(S_r)$ 11 or 12 suggests that some structural rearrangement of the coal matrix must occur during this phase of maturation too, given that oxygen-suppression of the C signal from the FID during Rock-Eval analysis does not appear to be able to account for the entire HI increase (Killops et al., 1998). However, it is not manifested in significant changes in bulk kinetic parameters in the same way as the jump in the transformation envelopes between $\text{Rank}(S_r)$ 12 and 13 ($\text{Rank}(S) \sim 12.5$ – 13.5). It is unclear whether the same structural rearrangement involving retained bitumen is at work, with the retained bitumen masking its effects on the HI transformation kinetics.

The Tara coals were solvent extracted and then thermally extracted before kinetic analysis in order to minimize the effects of retained bitumen. The presence of adsorbed bitumen may affect the optimised kinetics obtained from open-system pyrolysis, at least by extending the E_{act} distribution to lower values than if no bitumen were present. Solvent extraction on its own is not sufficient to remove the most strongly adsorbed bitumen and subsequent thermal extraction is able to remove further significant amounts of hydrocarbons (Radke, Willsch, Leythaeuser, & Teichmüller, 1982), as was verified by thermal-extraction high-resolution GC analysis of one of the Tara coal samples. The maximum temperature that can be used for thermal extraction without causing cracking of the kerogen structure depends on the maturity of the sample. For the samples used in this study it was considered that the maximum safe temperature was 250 °C, but this may not have been sufficiently high to ensure removal of all adsorbed components (Béhar, Tang, & Liu, 1997). It is possible that adsorbed bitumen plays an important role in the observed bulk kinetics. This bitumen could be related to the ‘neokerogen’ of Schenk and Horsfield (1998). It is conceivable that the early stages of HI transformation involve the cleavage of asphaltene-like material, which is effectively retained within the coal matrix but is liberated during pyrolysis. This could account for the lack of decrease in HI but the anomalous shift to lower temperature in the transformation-rate envelopes of samples 8 and 9 ($\text{Rank}(S_r) \sim 12.5$). As catagenesis progresses the asphaltene-like fragments would tend to break down further and become more readily expelled. Flushing of such material is

likely to be most extensive at the onset of significant paraffin expulsion, believed to occur at $\text{Rank}(S_r) \sim 12.5$ in the Tara coals, and would effectively switch off any further alteration, as suggested by the subsequent lack of change in the transformation-rate envelopes.

The effect of the jump in transformation-rate envelopes between samples 10 and 11 observed in Fig. 8 can be evaluated by using the kinetic parameters for these two coals to predict the amount of oil generated from the cumulative thickness of Cretaceous coals encountered in Tara-1 (325 m; Funnell & Allis, 1997). Assuming an average density of 1.35 g cm^{-3} and C_{org} content of 70% for the coal, and an oil density of 0.8 g cm^{-3} , some 0.59×10^6 bbls per hectare are predicted to have been generated according to coal 10 kinetics, but only 0.16×10^6 bbls from coal 11 kinetics. Tara-1 was drilled on a structural high, so the amounts of oil per hectare generated and expelled in the kitchen area would be considerably greater.

Further comparison of the kinetics of coals 10 and 11 can be made by their application to the thermal history of coal 16. The resulting maturation trends are shown in Fig. 12, together with that derived from coal 2 kinetics. The coal 10 kinetics result in a considerably greater extent of kerogen conversion than those of coal 11. Differences in the timing of the onset of oil expulsion can also be investigated using Fig. 12, but firstly it is necessary to give some consideration to the oil-expulsion threshold. Whether coals can expel oil is still the subject of some debate (Katz, 1994), and so predicting general guidelines for expulsion thresholds is problematical. Diffusion-based models of expulsion have no expulsion thresholds per se (Stainforth & Reinders, 1990), whereas adsorption-based models suggest a threshold of $\sim 0.1 \text{ gHC g C}_{\text{kerogen}}^{-1}$, although with the possibility of significant variations for some coals (Pepper & Corvi, 1995; Sandvik, Young, & Curry, 1992). S1/TOC data for the Tara coals suggest an expulsion

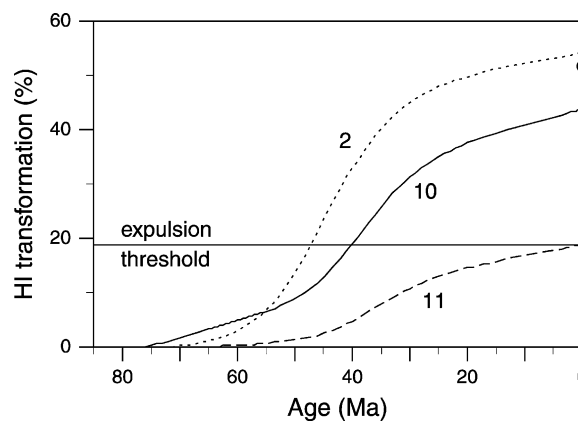


Fig. 12. Predicted maturation paths for coal 16 based on thermal model in Fig. 5, using discrete- E_{act} free-A data for coal samples 2, 10 and 11 (Table 1). Solid point = present HI conversion for coal 16, based on normalised HI value of $150 \text{ mgHC g C}_{\text{org}}^{-1}$. Oil-expulsion threshold ($\sim 55 \text{ mgHC g C}_{\text{org}}^{-1}$) is equivalent to $\sim 19\%$ HI conversion for coal 2.

threshold of $\sim 0.03 \text{ gHC g C}_{\text{kerogen}}^{-1}$ (Fig. 2). If an expulsion threshold of $0.1 \text{ g oil per g C}_{\text{kerogen}}$ is assumed, which equates to conversion of $100 \text{ mgHC g C}_{\text{org}}^{-1}$, 35% of the normalised HI of coal 2 must be transformed, providing the first 35% is virtually entirely oil. In Tara-1 well expulsion appears to begin at a maturity approaching that of coal 11, for which coal 2 kinetics predict an HI conversion of $\sim 19\%$, equating to $\sim 55 \text{ mgHC g C}_{\text{org}}^{-1}$. GOGI values for oil-prone NZ coals like the Tara coals are typically 0.4, so the oil potential of coal 2 is likely to be $\sim 200 \text{ mgHC g C}_{\text{org}}^{-1}$, suggesting the adsorption threshold can be exceeded and expulsion of oil occurs even using relatively conservative criteria. Using the threshold suggested by the Tara-1 data of $55 \text{ mg oil per g C}_{\text{kerogen}}$, Fig. 12 shows that the expulsion threshold would be exceeded by $\sim 40 \text{ Ma}$ applying coal 10 kinetics to coal 16, but at only 1 Ma using coal 11 kinetics, compared with 47 Ma using the coal 2 kinetics.

Although coals 10 and 11 are only some 150 m apart, and hence of similar maturity, the difference in kinetic parameters between these two coals clearly has significant implications for the amounts of oil generated and the timing of expulsion under typical geological conditions. Despite the problems of adsorption and restructuring, the kinetic parameters for coal 2 appear to reproduce the observed, corrected, HI trend of the Tara coals reasonably accurately (Fig. 7). Whether this is fortuitous, or whether coals of $\text{Rank}(S_r) \sim 8.5$ in general have this property is not known at present. However, it should be noted that the coal 2 kinetics tend to underestimate normalised HI transformation slightly at low-maturity and to overestimate it slightly at high maturity (Fig. 7(b)). This could potentially result from the optimisation programme tending to average out the influence of the most and least readily released hydrocarbons on the overall kinetic parameters. One effect would be that the influence of the higher bond-dissociation energies only becomes apparent after the onset of oil expulsion releases most of the adsorbed components, accounting for at least some of the shift in transformation-rate envelopes between samples 10 and 11 in Fig. 8. The apparently aberrant behaviour of the transformation-rate envelopes of samples 8–10, which contain the greatest quantities of adsorbed/trapped components, may be similarly explained. Although the above modelling is based on the kinetics of bulk kerogen conversion as measured by HI, compositional kinetics must also be affected.

5. Conclusions

The maturity-related changes in the HI transformation-rate envelopes for a suite of compositionally related Late Cretaceous–Paleocene coals from Tara-1 well, Great South Basin, New Zealand, are consistent with those previously reported for Carboniferous German coals (Schenk & Horsfield, 1998). Rather than a progressive migration of transformation-rate envelopes to higher temperature there is

a rapid transition with the $\text{Rank}(S_r)$ 12–13.5 range, which coincides with the proposed onset of significant paraffinic oil expulsion (Killops et al., 1998). An artificially matured sample did not yield kinetic parameters that could reproduce the transformation-rate envelopes of the naturally matured samples. This behaviour has been noted in other studies and can be attributed to the influence of heating rate on competing reactions, particularly the extent of solid-state aromatisation (Schenk & Horsfield, 1998). Structural rearrangement during natural maturation appears at least partially responsible for changes in the kinetics of HI transformation.

The effects of structural rearrangements over the $\text{Rank}(S_r)$ range ~ 10 – 11 (samples 4–7), some or all of which are responsible for the observed increase in HI, are not manifested in significant changes in HI transformation kinetic parameters. Similarly, the lack of major changes in the transformation-rate envelopes at higher rank suggests either that any further structural rearrangement does not produce a significant change in the A and E_{act} distribution of hydrocarbon-generating bonds, or that the expulsion of oil drastically reduces the degree of further rearrangements involving hydrocarbon-generating moieties within the kerogen.

The behaviour of the transformation-rate envelopes at intermediate maturity, in the rank range associated with the onset of significant hydrocarbon generation and subsequent expulsion ($\text{Rank}(S_r) \sim 11$ – 13.5), may be explained primarily by the influence of adsorbed bitumen on the ‘average’ A value obtained from discrete-energy kinetic modelling. Initially this material is unlikely to be readily expelled or removed by thermal extraction at moderate temperatures, but is released during Rock-Eval analysis at temperatures $> 300 \text{ }^\circ\text{C}$ but which are still lower than those involved in cracking of the residual macromolecular matrix that accounts for the rest of the S_2 signal. However, as catagenetic cracking proceeds and significant expulsion of hydrocarbons occurs, the bulk of the previously adsorbed bitumen is probably released and the low-energy (high A) weighting of this fraction is no longer factored into the kinetic optimisation.

It is apparent that kinetic parameters for immature coals are not ideal for modelling the whole phase of hydrocarbon generation. Nevertheless, the bulk HI transformation kinetics for the least mature Tara coal, of $\text{Rank}(S_r) \sim 8.5$, does appear to predict the observed changes in normalised HI values that have been corrected for the apparent suppression of HI at $\text{Rank}(S_r)$ values < 11 , with only slight overestimation of kerogen conversion at the lower maturities of the rank range examined and slight underestimation at the higher maturities. Increasing underestimation of kerogen conversion above $\text{Rank}(S_r) \sim 15$ could prove problematical. Whether the apparent accuracy of modelled HI transformation is fortuitous in the example of the Tara coals or whether it applies generally to oil-prone coals has yet to be confirmed. Because the oils expelled by coals are paraffinic with a high n -alkane content, a suitable approach

may be to base modelling of the amount of expelled oil on the kinetics of *n*-alkane generation, and the expulsion timing on the kinetics of aromatic and polar component generation, once the potential effects of structural rearrangements on the associated kinetics have been investigated. Clearly, caution must be exercised when choosing the most appropriate coal samples upon which to base maturity models, in terms of both measurable oil potential and kerogen-conversion kinetics.

Acknowledgements

We are grateful to the Foundation for Research, Science, Technology, NZ, for supporting this research (contract number C05806), To Jean-Paul Boudou of Université Pierre et Marie Curie (Paris, France) for Rock-Eval analyses, and to Pat Suggate of IGNS (Lower Hutt, New Zealand) for his helpful comments on the manuscript. IGNS publication number 2562.

References

- Alpern, B. (1966). Un exemple intéressant de houillification dans le bassin Lorrain et ses prolongements. In G. D. Hobson (Ed.), *Advances in organic geochemistry 1964* (pp. 129–145). Oxford: Pergamon Press.
- Armstrong, P. A., Chapman, D. S., Funnell, R. H., Allis, R. G., & Kamp, P. J. J. (1996). Thermal modelling and hydrocarbon generation in an active-margin basin: Taranaki Basin, New Zealand. *American Association of Petroleum Geologists Bulletin*, 80, 1216–1241.
- Béhar, F., Tang, Y., & Liu, J. (1997). Comparison of rate constants for some molecular tracers generated during artificial maturation of kerogens: Influence of kerogen type. *Organic Geochemistry*, 26, 281–287.
- Boreham, C. J., Horsfield, B., & Schenk, H. J. (1999). Predicting the quantities of oil and gas generated from Australian Permian coals, Bowen Basin using pyrolytic methods. *Marine and Petroleum Geology*, 16, 165–188.
- Bostick, N. H., & Daws, T. A. (1994). Relationships between data from Rock-Eval pyrolysis and proximate, ultimate, petrographic, and physical analyses of 142 diverse US coal samples. *Organic Geochemistry*, 21, 35–49.
- Boudou, J.-P., Espitalié, J., Bimer, J., & Salbut, P. D. (1994). Oxygen groups and oil suppression during coal pyrolysis. *Energy and Fuels*, 8, 972–977.
- Burnham, A. K., & Sweeney, J. J. (1989). A chemical model of vitrinite maturation and reflectance. *Geochimica et Cosmochimica Acta*, 53, 2649–2657.
- Cook, R. A., Sutherland, R., Zhu, H., et al. (1999). *Cretaceous-Cenozoic geology and petroleum systems of the Great South Basin, New Zealand. Institute of Geological and Nuclear Sciences Monograph 20*, Lower Hutt, New Zealand: Institute of Geological and Nuclear Sciences.
- Dickinson, W. W., Newman, R. H., & Collen, J. D. (1991). *Maturation parameters measured from ¹³C NMR spectra compiled from Upper Cretaceous and Tertiary coals, New Zealand. Geology Board of Studies Publication 9*, New Zealand: Victoria University of Wellington.
- Durand, B., & Paratte, M. (1983). Oil potential of coals: A geochemical approach. J. Brooks (Ed.), *Petroleum Geochemistry and exploration of Europe. Geological Society Special Publication*, 12, pp. 255–265.
- Francis, W. (1952). The evaluation and classification of coals from Commonwealth sources. *Journal of the Institute of Fuel*, 24, 15–78.
- Funnell, R. H., & Allis, R. G. (1997). *Hydrocarbon maturation potential of offshore Canterbury and Great South basins. 1996 New Zealand Petroleum Conference Proceedings*, Wellington, New Zealand: Ministry of Commerce, pp. 22–30.
- Hunt International Petroleum (1978). *Well completion report, Tara-1, Great South Basin, New Zealand. Petroleum Report 732*. Wellington, New Zealand: Ministry of Commerce.
- Jarvie, D. M. (1991). Factors affecting Rock-Eval derived kinetic parameters. *Chemical Geology*, 93, 79–99.
- Jarvie, D. M., & Lundell, L. L. (2001). In C. M. Isaacs, & J. Rullkotter (Eds.), *Amount, type, and kinetics of thermal transformation of organic matter in the Miocene Monterey Formation* (pp. 268–295). *The Monterey Formation: From rocks to molecules*, New York: Columbia University Press.
- Karayigit, A. I., & Whateley, M. K. G. (1997). Properties of a lacustrine subbituminous (k1) seam, with special reference to the contact metamorphism, Soma-Turkey. *International Journal of Coal Geology*, 34, 131–155.
- Katz, B. J. (1994). An alternative view on Indo-Australian coals as a source of petroleum. *APEA Journal*, 256–267.
- Killops, S. D., Allis, R. G., & Funnell, R. H. (1996). Carbon dioxide generation from coals in Taranaki Basin, New Zealand: Implications for petroleum migration in southeast Asian Tertiary basins. *American Association of Petroleum Geologists Bulletin*, 80, 545–569.
- Killops, S. D., Cook, R. A., Sykes, R., & Boudou, J.-P. (1997). Petroleum potential and oil-source correlation in the Great South and Canterbury basins. *New Zealand Journal of Geology and Geophysics*, 40, 405–423.
- Killops, S. D., Funnell, R. H., Suggate, R. P., Sykes, R., Peters, K. E., Walters, C., Woolhouse, A. D., Weston, R. J., & Boudou, J.-P. (1998). Predicting generation and expulsion of paraffinic oil from vitrinite-rich coals. *Organic Geochemistry*, 29, 1–21.
- Killops, S. D., Raine, J. I., Woolhouse, A. D., & Weston, R. J. (1995). Chemostratigraphic evidence of higher-plant evolution in the Taranaki Basin, New Zealand. *Organic Geochemistry*, 23, 429–445.
- Michelsen, J. K., & Khorasani, G. K. (1995). The kinetics of thermal degradation of individual oil-generating macerals: Calibration with microscopical fluorescence spectrometry and bulk flow pyrolysis. *Organic Geochemistry*, 22, 179–189.
- Pepper, A. S., & Corvi, P. J. (1995). Simple kinetic models of petroleum formation. Part III. Modelling an open system. *Marine and Petroleum Geology*, 12, 417–452.
- Radke, M., Willsch, H., Leythaeuser, D., & Teichmüller, M. (1982). Aromatic components of coal: Relation of distribution pattern to rank. *Geochimica et Cosmochimica Acta*, 46, 1831–1848.
- Raine, J. I. (1984). *Outline of a palynological zonation of Cretaceous to Paleogene terrestrial sediments in West Coast Region, South Island, New Zealand. New Zealand Geological Survey Report 109*, Lower Hutt, New Zealand: Institute of Geological and Nuclear Sciences.
- Rogers, J., Suggate, R. P., Elphick, J. O., & Ross, J. B. (1962). Metamorphism of a lignite. *Nature*, 195, 1078–1080.
- Rouzaud, J. N., Geuchchati, N., Kister, J., & Conard, J. (1991). Structural characterisation of coalification: Example of Gironville borehole. *Bulletin de la Société Géologique de France*, 162, 201–209.
- Sandvik, E. I., Young, W. A., & Curry, D. J. (1992). Expulsion from hydrocarbon sources: The role of organic absorption. *Organic Geochemistry*, 19, 77–87.
- Schenk, H. J., & Horsfield, B. (1998). Using natural maturation series to evaluate the utility of parallel reaction kinetic models: An investigation of Toarcian shales and Carboniferous coals, Germany. *Organic Geochemistry*, 29, 137–154.
- Schopf, J. M., & Long, W. E. (1966). Coal metamorphism and igneous associations in Antarctica. In R. F. Gould (Ed.), *Coal science*

- (pp.w 156–195). *Advances in Chemistry Series No. 55*, American Chemical Society.
- Stainforth, J. G., & Reinders, J. E. A. (1990). Primary migration of hydrocarbons by diffusion through organic matter networks. *Organic Geochemistry*, 16, 61–74.
- Suggate, R. P. (1959). *New Zealand coals: Their geological setting and its influence on their properties*. New Zealand Department of Scientific and Industrial Research Bulletin 134, Lower Hutt, New Zealand: Institute of Geological and Nuclear Sciences.
- Suggate, R. P. (2000). The Rank(S_r) scale: Its basis and its applicability as a maturity index for all coals. *New Zealand Journal of Geology and Geophysics*, 43, 521–553.
- Suggate, R. P. (2002). Application of Rank(S_r), a maturity index based on chemical analyses of coals. *Marine and Petroleum Geology*, 19, 929–950.
- Suggate, R. P., & Boudou, J.-P. (1993). Coal rank and type variation in Rock-Eval assessment of New Zealand coals. *Journal of Petroleum Geology*, 16, 73–88.
- Sweeney, J. J., & Burnham, A. K. (1990). Evaluation of a simple model of vitrinite reflectance based on chemical kinetics. *American Association of Petroleum Geologists Bulletin*, 74, 1559–1570.
- Sykes, R., Suggate, R. P., Funnell, R. H., Boudou, J. P., Killops, S. D., Cook, R. A., & Newman, J. (1998). Petroleum generation and expulsion from coals and coaly shales in Tara-1, Great South Basin, New Zealand: Facies controls, maturity thresholds and expulsion history. *Handbook and Abstracts, International Conference on Coal Seam Gas and Oil, Brisbane, Australia*, 22.
- Sykes, R., Suggate, R. P., & King, P. R. (1991). *Timing and depth of maturation in southern Taranaki Basin from reflectance and Rank(S_r)*. *Proceedings of the 1991 New Zealand Oil Exploration Conference*, Wellington: Ministry of Commerce, pp. 373–389.
- Teichmüller, M., & Durand, B. (1983). Fluorescence microscopical rank studies on liptinites and vitrinites in peat and coals, and comparison with results of the Rock-Eval pyrolysis. *International Journal of Coal Geology*, 2, 197–230.